Los Alamos
NATIONAL LABORATORY
EST. 1943

LA-UR-15-21616
Approved for public release; distribution is unlimited.

Title:	An Exact, Compressible One-Dimensional Riemann Solver for General, Convex Equations of State
Author(s):	Kamm, James Russell
Intended for:	Report
Issued:	2015-03-05

Disclaimer:
Los Alamos National Laboratory, an affirmative action/equal opportunity employer,is operated by the Los Alamos National Security, LLC for the National NuclearSecurity Administration of the U.S. Department of Energy under contract DE-AC52-06NA25396. By approving this article, the publisher recognizes that the U.S. Government retains nonexclusive, royalty-free license to publish or reproduce the published form of this contribution, or to allow others to do so, for U.S. Government purposes. Los Alamos National Laboratory requests that the publisher identify this article as work performed under the auspices of the U.S. Departmentof Energy. Los Alamos National Laboratory strongly supports academic freedom and a researcher's right to publish; as an institution, however, the Laboratory does not endorse the viewpoint of a publication or guarantee its technical correctness.

An Exact, Compressible One-Dimensional Riemann Solver for General, Convex Equations of State

James R. Kamm

Abstract

This note describes an algorithm with which to compute numerical solutions to the one-dimensional, Cartesian Riemann problem for compressible flow with general, convex equations of state. While high-level descriptions of this approach are to be found in the literature, this note contains most of the necessary details required to write software for this problem. This explanation corresponds to the approach used in the source code that evaluates solutions for the 1D, Cartesian Riemann problem with a JWL equation of state in the ExactPack package [16, 29]. Numerical examples are given with the proposed computational approach for a polytropic equation of state and for the JWL equation of state.

1. Governing Equations for Compressible Flow

The Euler equations describing the conservation of mass, momentum, and energy for a compressible fluid can be written in conservation form as [6, 31]:

$$\frac{\partial \rho}{\partial t} + \frac{\partial (\rho u)}{\partial x} = 0 \,, \tag{1}$$

$$\frac{\partial (\rho u)}{\partial t} + \frac{\partial (\rho u^2 + p)}{\partial x} = 0 \,, \tag{2}$$

$$\frac{\partial (\rho E)}{\partial t} + \frac{\partial [u(\rho u^2 + p)]}{\partial x} = 0 \,. \tag{3}$$

Cartesian geometry is assumed with spatial coordinate x, ρ is the mass density, u is the velocity, p is the pressure, and $E \coloneqq e + \frac{1}{2}u^2$ is the specific total energy with e the specific internal energy (SIE). The working fluid is an inviscid, non-heat conducting, non-radiating, non-reactive gas, for which the mass density, pressure, and SIE are related through an (incomplete) equation of state (EOS), expressed as

$$p = \mathcal{P}(\rho, e) \quad \text{or} \quad e = \mathcal{E}(\rho, p) \,. \tag{4}$$

The further assumption is made that the EOS describing the fluid is convex, i.e., that the fundamental derivative $\mathcal{G}$ is strictly positive[1] [25, 31, 32]; this assumption is appropriate for many gases. From the EOS, the square of the corresponding sound speed, a^2, is related to the variations of pressure, density, and SIE as

$$a^2 \coloneqq \left(\frac{\partial p}{\partial \rho}\right)_s \quad \Rightarrow \quad a^2 = \left(\frac{\partial \mathcal{P}}{\partial \rho}\right)_e + \frac{p}{\rho^2}\left(\frac{\partial \mathcal{P}}{\partial e}\right)_\rho \tag{5}$$

$$\Leftrightarrow \quad a^2 = \left[\frac{p}{\rho^2} - \left(\frac{\partial \mathcal{E}}{\partial \rho}\right)_p\right] \Big/ \left(\frac{\partial \mathcal{E}}{\partial p}\right)_\rho \,, \tag{6}$$

where s is the entropy. For later use, the functional dependence of the sound speed on the density and pressure is denoted as:

$$a = \mathcal{A}(\rho, p) \; . \tag{7}$$

The conservation laws in Eqs. (1–3) can be rewritten in characteristic form [5, 19] as:

$$du - \frac{dp}{\rho a} = 0 \qquad \text{along} \qquad dx - (u - a)\, dt \quad = 0 \; , \tag{8}$$

$$d\rho - \frac{dp}{a^2} = 0 \qquad \text{along} \qquad dx - u\, dt \qquad = 0 \; , \tag{9}$$

$$du + \frac{dp}{\rho a} = 0 \qquad \text{along} \qquad dx - (u + a)\, dt \quad = 0 \; , \tag{10}$$

This form of the equations illuminates the structure of the solution to the 1D Riemann problem (defined below), is useful for describing simple waves, and is particularly helpful for understanding wave structure in the (p, u)-plane.[2]

2. The 1D Riemann Problem for Compressible Flow

The 1D Riemann problem for compressible flow describes the time-dependent evolution of an initial discontinuity between two semi-infinite, uniform states. The literature on this subject is vast, and the interested reader is directed to the following general references for additional details: [6, 23, 24, 25, 31, 33, 34]. The compressible media on the two sides of the initial discontinuity may be described by the same EOS or by different EOSs. Under these assumptions, a self-similar flow evolves, i.e., assuming (without loss of generality) that the initial discontinuity is at the origin, the solution is solely a function of x/t. Additionally, the assumption of convex EOSs excludes the possibility of non-standard flow structures (i.e., rarefaction shock fronts and isentropic compression waves).[3] With these assumptions, it can be shown that the time-dependent solution to the Riemann problem must consist of a contact discontinuity and a combination of (expansive) rarefaction waves and (compressive) shock fronts. [6, 21, 25, 33]

The Riemann problem initial conditions include a discontinuity, which is manifested as the contact discontinuity in the evolving flow. The contact has several features that distinguish it from either a shock front or a rarefaction wave. Physically, the contact is the sole wave across which there is no mass flux, i.e., no flow of material. Like a shock front, the states on either side of the contact discontinuity are uniform; this spatial uniformity holds until the next wave is reached. Unlike a shock, however, across the contact both pressure and velocity do not change; this is not true of other flow quantities, such as density and SIE. It is this equality of the pressure and velocity across the contact that provides the key to the overall numerical solution.

The other two families of possible waves also have properties that guide the corresponding numerical solutions. Shock fronts correspond to compressions and are flow discontinuities across which there is a non-zero mass flux, unlike a contact; there is also a jump in entropy across a shock wave, in distinction to a rarefaction.[4] The Rankine-Hugoniot (RH) equations [18, 19, 33, 41] codify the conditions that ensure the conservation of mass flux, momentum flux, and energy flux in the direction normal to a

discontinuity surface in the material. The RH equations across a shock front can be expressed in the following form in a frame in which the initial states and the shock each may have non-zero velocity:

$$\rho^{\otimes}\,(\mathcal{U}_{\mathcal{S}} - u^{\otimes}) = \rho^{\odot}\,(\mathcal{U}_{\mathcal{S}} - u^{\odot})\,, \tag{11}$$

$$\rho^{\otimes}\,(\mathcal{U}_{\mathcal{S}} - u^{\otimes})^2 + p^{\otimes} = \rho^{\odot}\,(\mathcal{U}_{\mathcal{S}} - u^{\odot})^2 + p^{\odot}\,, \tag{12}$$

$$e^{\otimes} + (p^{\otimes}/\rho^{\otimes}) + \frac{1}{2}\,(\mathcal{U}_{\mathcal{S}} - u^{\otimes})^2 = e^{\odot} + (p^{\odot}/\rho^{\odot}) + \frac{1}{2}\,(\mathcal{U}_{\mathcal{S}} - u^{\odot})^2\,, \tag{13}$$

where $\mathcal{U}_{\mathcal{S}}$ is the shock speed, "$\odot$" denotes the pre-shock state (i.e., ahead of the shock), and "$\otimes$" denotes the post-shock state (i.e., behind the shock).[5] These equations can be written compactly as the jump conditions

$$[\![\, \rho\,(\mathcal{U}_{\mathcal{S}} - u)\,]\!] = 0\,, \tag{14}$$

$$[\![\, \rho\,(\mathcal{U}_{\mathcal{S}} - u)^2 + p\,]\!] = 0\,, \tag{15}$$

$$[\![\, e + (p/\rho) + \frac{1}{2}(\mathcal{U}_{\mathcal{S}} - u)^2\,]\!] = 0\,, \tag{16}$$

where the bracket represents the jump in the enclosed quantity, i.e., $[\![\,\Theta\,]\!] \coloneqq \Theta^{\otimes} - \Theta^{\odot}$. If there is a shock front in the evolving flow, the RH conditions provide the basis for the numerical evaluation of the post-shock state.

Unlike shock fronts, rarefaction waves correspond to expansions, have finite spatial extent, and are isentropic, with pressure that is monotone and continuous through the wave. One implication of these conditions is that the characteristic equations can be reduced to the following ODEs through the rarefaction:

$$\frac{dp}{d\rho} = a^2 = \mathcal{A}^2(\rho, p(\rho)) \qquad \text{and} \qquad \frac{du}{d\rho} = \pm\,\frac{a}{\rho}\,. \tag{17}$$

In these equations, the reduction of the sound speed to a function of density only is a result of the isentropic condition. In the second equation, the sign depends on whether the rarefaction is left-facing ($-$) or right-facing ($+$).[6] The ODEs in Eq. (17) provide the basis for evaluating the numerical solution for the entire flow state at all locations through the rarefaction wave.

If one excludes the possibility of vacuum initial conditions, then the five possible wave combinations of the evolving self-similar flow (named according to the waves present, from left to right) are [14]:

1. Shock-Contact-Shock (SCS)
2. Shock-Contact-Rarefaction (SCR)
3. Rarefaction-Contact-Rarefaction (RCR)
4. Rarefaction-Contact-Shock (RCS)
5. Rarefaction-Contact-Vacuum-Contact-Rarefaction (RCVCR)

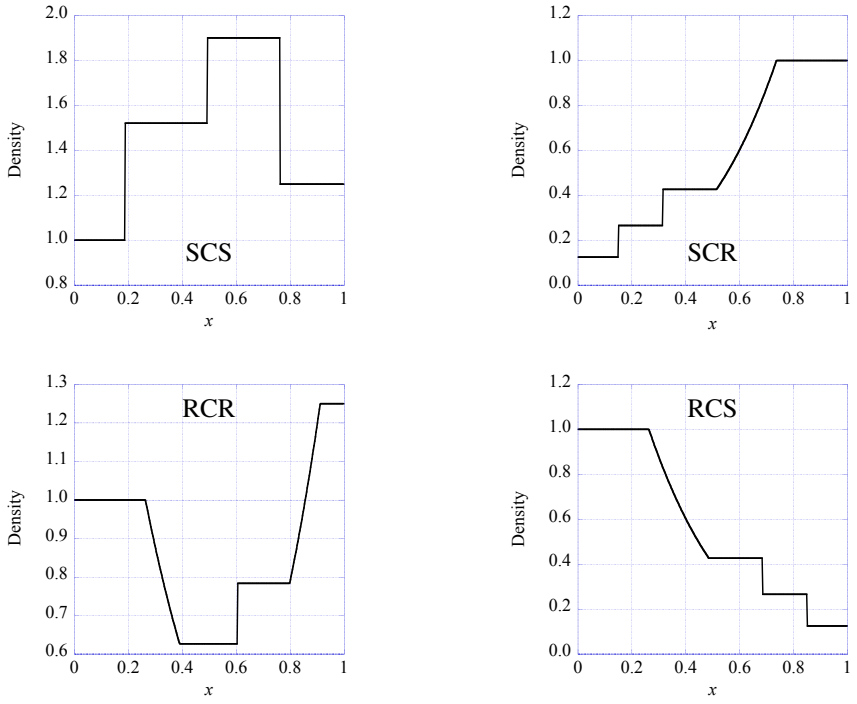

Figure 1: Snapshots of density versus position for examples of four of the five possible wave combinations of the 1D Riemann problem solution for the gas dynamics equations with a general, convex EOS. Clockwise from the upper left: Shock-Contact-Shock (SCS); Shock-Contact-Rarefaction (SCR); Rarefaction-Contact-Shock (RCS); and Rarefaction-Contact-Rarefaction (RCR).

For given EOSs, the initial conditions determine which one of these flow structures develops. The numerical scheme described in the following computes solutions for the first four. Snapshots of the density fields for these four cases are plotted in Fig. 1; for snapshots of the other flow fields in the RCS case, see Fig. 2.

3. Overview of the Solution Approach to the 1D Riemann Problem

As previously mentioned, specifics of the wave structure suggest how the numerical solution can be calculated. In the case of polytropic gases, many of the associated relations can be evaluated in closed form, as described, e.g., in [14, 33]; in the general EOS case, several of these relations must be solved numerically. The polytropic gas case, however, still requires the numerical solution of a single nonlinear equation.[7]

To obtain the numerical solution for the case of general convex EOSs, further computational complexity is unavoidable. Different approaches been proposed by different authors, several of which are mentioned by Gottlieb and Groth [14]. The work of

Colella and Glaz [5] is a key reference, describing previous work and providing a complete solution procedure. Other researchers, e.g., [2, 10, 20, 22, 27], either based their Riemann solvers on this solution strategy or took slightly different approaches.[8]

The key property exploited in the overall numerical solution is the equality of the pressure and velocity across the contact discontinuity. Immediately adjacent to the contact wave is the "star-state" region, throughout which the pressure and velocity are equal and uniform. It is referred to as the star-state for the superscript that is commonly used to identify these pressure $p^\star$ and velocity $u^\star$ values. The flow states in this region are related to the initial uniform states to the left (L) and to the right (R) through waves that must be either shocks or rarefactions. A synopsis of the iterative procedure with which to evaluate the entire solution is given as: estimate the star-state pressure; determine the corresponding complete left and right star-states; use the mismatch in the computed left and right star-state velocities to update the estimate of the star-state pressure; iterate this loop to a predetermined tolerance in the discrepancy between left and right star-state velocities; and, upon convergence, compute the full solution from the converged star-state pressure and velocity.

Many details are required to turn this high-level description into an algorithm that can be instantiated in software. A preliminary refinement of this approach into the following pseudocode hints at the additional complexity:

I. Select the overall iteration scheme to be used to calculate the solution.

   a. The equality of the pressure and velocity across the contact discontinuity must be fashioned into nonlinear equations to be solved numerically.

II. Provide initial estimates of star-state pressure, $p^{\star(0)}$, and velocity $u^{\star(0)}$.

   a. These values are typically estimated using the acoustic approximation, i.e., employing the sound speeds of the initial uniform left and right states.

   b. Depending upon the overall iteration scheme used, an additional initial estimate of the star-state quantities may be required.

III. Using the approximate star-state pressure, determine whether the wave connecting the uniform state (for both the left and right states) and the corresponding star-state is a shock or a rarefaction; for $\ell = L, R$:

   a. $p^{\star(k)} > p_\ell \Rightarrow$ shock: use the RH conditions of Eqs. (11–13) to determine the complete, post-shock star-state corresponding to $p^{\star(k)}$; for a general EOS, this involves finding the zero of a single nonlinear equation, which involves several EOS calls.

   b. $p^{\star(k)} \leq p_\ell \Rightarrow$ rarefaction: use the adiabatic conditions of Eq. (17) to determine the complete, post-rarefaction star-state corresponding to $p^{\star(k)}$; for a general EOS, this involves (i) finding the zero of a single nonlinear equation and (ii) numerically integrating the ODEs for the solution through the rarefaction, each of which involve many EOS calls.

   c. Depending upon the overall iterative solution scheme used, this procedure may be used to provide an additional initial iterate, i.e., $p^{\star(1)}$ and $u^{\star(1)}$.

IV. At the kth iteration, evaluate the discrepancy between the computed left and right star-state velocities, $u_L^{\star(k)}$ and $u_R^{\star(k)}$ and possibly evaluate the next star-state estimate.

   a. If this value is less than the allowed error tolerance, then evaluate the complete left and right star-state solutions and proceed to step V.

   b. Else use the velocity mismatch to obtain the next iterative estimate of the star-state pressure $p^{\star(k+1)} \leftarrow p^{\star(k)}$ and return to step III.

V. When a sufficiently accurate estimate of the star-state solution is calculated (i.e., case IVa obtains), then values of the complete Riemann problem solution at any point in the domain can be evaluated; this process may involve interpolation to specified spatial positions of the iteratively-determined solution (specifically in the rarefaction(s), if present).

There are several numerical procedures that must be implemented in this approach.

- Finding reasonable initial estimates of the star-state pressure and velocity: to start the overall iterative solution loop, values for these quantities are required, and the simple acoustic approximation, alone, may not provide adequate estimates for highly nonlinear EOSs.

- Finding the zero of a single nonlinear equation: this is most effectively accomplished when the root can be bracketed (i.e., when one has two abscissæ that give function values of opposite sign), which, given the complexity of these equations and nonlinear EOSs, may not be immediately obvious. The root-finding routing used was the well-known scalar root finding routine ZEROIN of Forsythe, Malcolm, and Moler [9].[9]

- Numerical integrating an ODE: for the (generally) smooth functions considered, this should not present problems; however, it is conceivable that the computational evaluation for a complex analytic EOS could pass through "forbidden" areas of the EOS, where, e.g., the SIE or the square of the sound speed is negative. The numerical integration scheme used was a fourth-order Runge Kutta routine, as suggested by Banks [2] and described in §III(b).

- Interpolating solution values at specified positions: this would be necessary through any rarefaction, which, being smooth, should not present problems for even simple interpolation routines. This was accomplished with the cubic spline routines SPLINE and SEVAL of Forsythe, Malcolm, and Moler [9].

Since finding the zeroes of the nonlinear equations and numerically solving ODEs each involve an appreciable number of EOS calls (say, hundreds or thousands), this approach, while accurate, is prohibitively inefficient as the Riemann solver for a general compressible flow algorithm; even the algorithmically much less complex polytropic gas Riemann solver is impractical for general compressible flow codes. When an exact solution is to be used for code verification, however, this concern is essentially

irrelevant, as the hydrocode calculations being assessed typically require significantly greater resources than the exact Riemann problem solution evaluation.

4. Details of the Solution Approach to the 1D Riemann Problem

In this section we describe in detail the solution scheme. Recall that the 1D Riemann problem describes the evolution of either the same material or two different materials separated by a massless discontinuity, i.e., the EOSs on the two sides of the initial discontinuity can be different. The solution scheme described in the following is appropriate for this general case. The approach presented combines elements of the methods outlined in [2, 5, 10, 22, 27].

I. The Overall Iteration Scheme

The overall iteration scheme is the secant method for determining the zero of a scalar function, as advocated by Colella & Glaz [5].[10] This method requires two initial estimates of the root, which, together with the function values at those points, determine the secant line. The subsequent estimates of the root follow from the function evaluations based on the zeroes of the secant line; see [39]. The convergence of the secant method is greater than linear, but not quadratic like Newton's method; unlike that method, however, the secant method requires only function values and no derivatives.

For the case at hand, the argument of the function f whose root will be found is the star-state pressure, $p^\star$, which is equal on both sides of the contact discontinuity. The function f is assigned to be the difference between the corresponding values of the velocity to the left and to the right of the contact, $u_L^\star$ and $u_R^\star$, at the specified pressure, i.e.,

$$f(p^\star) = u_L^\star(p^\star) - u_R^\star(p^\star)\,. \tag{18}$$

The iterative update of the pressure according to the secant method is:

$$p^{\star(k+1)} = p^{\star(k)} - f(p^{\star(k)}) \frac{p^{\star(k)} - p^{\star(k-1)}}{f(p^{\star(k)}) - f(p^{\star(k-1)})}\,. \tag{19}$$

As is clear from this relation, the secant method requires two initial estimates of the star-state pressure and star-state velocity difference. Note also that the secant method is not guaranteed to converge.

II. The Initial Estimate of the Star-State

Perhaps the simplest estimate of $p^\star$ is from the acoustic approximation. Following the development given by Toro (Eq. (9.28) in [33]), this estimate is given as:

$$p^{\star(0)} = [\, C_R\, p_L + C_L\, p_R + C_L\, C_R\, (u_L - u_R)\,] \,/\, (\, C_L + C_R\,)\ , \tag{20}$$

where the subscripts L and R refer to the left and right initial conditions, and C is the mass flux or Lagrangian wavespeed, given as $C := \rho\, a$, where a is the sound speed (i.e., acoustic velocity), associated with the respective initial conditions. This expression can be derived by integrating Eqs. (8) and (10) for p through the right and left waves, respectively, assuming that the Lagrangian wavespeed (i.e., ρa in the ODE

$dp/du = \pm\rho a$ through the right (+) and left (−) waves) is constant throughout the wave, with value equal to that in the corresponding uniform initial state.

Given the estimate of star-state pressure in Eq. (20) and the known initial condition pressures, the nature of the waves connecting the approximate star state to the left and right states is determined. The solution method for the other star-state quantities (including the velocity) depends on whether that wave is a shock or a rarefaction. Numerical schemes by which to calculate those solutions are explained in the next section. Using these procedures, one calculates the zeroth-iterate estimates of the velocity to the left of the contact, $u_L^{\star(0)}$, and to the right of the contact, $u_R^{\star(0)}$, and, thus, of $f(p^{\star(0)})$ from Eq. (18). With these estimates, one has values for all of the lowest-indexed quantities in the secant update, i.e., the values with superscript $(k-1)$ for $k = 1$ in Eq. (19).

One way to obtain the second estimate required for the secant method (i.e., the values with superscript (k) for $k = 1$ in Eq. (19)) is to use the same acoustic approximation, but with improved estimates of the Lagrangian wave speed based on the zeroth iterate values, as suggested by Fryxell et al. [10] More precisely, instead of using a value of Lagrangian wavespeed implied by the initial conditions, following Colella & Glaz [5] one defines a mean Lagrangian wavespeed $\overline{C}$ through these waves[11] that accounts for the wave structure. For the zeroth iterate and wave $\ell = L, R$, the mean Lagrangian wave speed is defined as:

$$\overline{C}_\ell^{(0)} := \begin{cases} \left| p^{\star(0)} - p_\ell \right| \Big/ \left| u_\ell^{\star(0)} - u_\ell \right| & \text{if} \quad u_\ell^{\star(0)} \neq u_\ell \,, \\ C_\ell = \rho_\ell \, a_\ell & \text{if} \quad u_\ell^{\star(0)} = u_\ell \,. \end{cases} \tag{21}$$

Using this value, a second, updated estimate for the star-state pressure can be obtained:

$$p^{\star(1)} = \left[\, \overline{C}_R \, p_L + \overline{C}_L \, p_R + \overline{C}_L \, \overline{C}_R \, (u_L - u_R) \, \right] \Big/ \left(\overline{C}_L + \overline{C}_R \right) \,, \tag{22}$$

With this value of $p^{\star(1)}$ one calculates, following the procedure described above for the zeroth iterate, the corresponding estimates of the velocity to the left of the contact, $u_L^{\star(1)}$, and to the right of the contact, $u_R^{\star(1)}$. These values are used to evaluate $f(p^{\star(k)})$ with $k = 1$ in Eq. (19). Thus, one has all values needed to begin the secant iteration.

III. Shock or Rarefaction Calculation

The relation between (i) the estimated star-state pressure at the kth iteration and (ii) the pressure in each of the uniform left (L) and right (R) initial states determines whether a shock front or a rarefaction wave connects those two states. These two cases require different approaches by which to calculate numerical solutions of the related equations.

III(a). *Shock Front Evaluation*

Consider first the case where $p^{\star(k)} > p_\ell$, $\ell = L, R$. This situation implies there is a shock front between the star-state and the initial uniform state. The RH equations specify the relation between the states ahead of and behind the shock. The lone post-shock value known, however, is $p^{\star(k)}$; consequently, one must evaluate the post-shock state through that material's EOS using $p^{\star(k)}$ and, say, some estimate of $\rho_\ell^{\star(k)}$. One can transform Eqs. (11–13) into the following scalar functions, each having abscissa of

the post-shock density, that must vanish identically across left-facing and right-facing shock fronts (see Banks [2], Eq. (3.2)).

Left shock jump relation:

$$\mathcal{S}_L(\rho_L^\star) = 0 = e_L + \frac{p_L}{\rho_L} + \frac{1}{2}\frac{\rho_L^\star}{\rho_L}\,\frac{p^{\star(k)} - p_L}{\rho_L^\star - \rho_L} - \left(e_L^\star + \frac{p^{\star(k)}}{\rho_L^\star} + \frac{1}{2}\frac{\rho_L}{\rho_L^\star}\,\frac{p^{\star(k)} - p_L}{\rho_L^\star - \rho_L}\right), \tag{23}$$

where $e_L^\star = \mathcal{E}_L(\rho_L^\star, p^{\star(k)})$ from the EOS for the left material.

Right shock jump relation:

$$\mathcal{S}_R(\rho_R^\star) = 0 = e_R + \frac{p_R}{\rho_R} + \frac{1}{2}\frac{\rho_R^\star}{\rho_R}\,\frac{p^{\star(k)} - p_R}{\rho_R^\star - \rho_R} - \left(e_R^\star + \frac{p^{\star(k)}}{\rho_R^\star} + \frac{1}{2}\frac{\rho_R}{\rho_R^\star}\,\frac{p^{\star(k)} - p_R}{\rho_R^\star - \rho_R}\right), \tag{24}$$

where $e_R^\star \coloneqq \mathcal{E}_R(\rho_R^\star, p^{\star(k)})$ from the EOS for the right material.

These nonlinear scalar equations must be solved numerically for $\rho_L^\star$ or $\rho_R^\star$, as required. This numerical solution procedure likely entails several EOS calls. With the star-state density and pressure, the SIE and sound speed can be evaluated through the EOS.

After one solves for post-shock densities satisfying these equations to some specified tolerance, the associated shock speeds can be evaluated according to the following relations (see Toro [33], §3.1.3):

$$\text{Left shock speed: } \mathcal{U}_{\mathcal{S},L} = u_L - \left[\left(\frac{\rho_L^\star}{\rho_L}\right)\left(\frac{p^\star - p_L}{\rho_L^\star - \rho_L}\right)\right]^{1/2}, \tag{25}$$

$$\text{Right shock speed: } \mathcal{U}_{\mathcal{S},R} = u_R + \left[\left(\frac{\rho_R^\star}{\rho_R}\right)\left(\frac{p^\star - p_R}{\rho_R^\star - \rho_R}\right)\right]^{1/2}, \tag{26}$$

where u_L and u_R are the particle velocities of the initial left and right states. These shock speeds are used to compute the corresponding post-shock particle velocities (also in Toro [33], §3.1.3):

$$\text{Left star velocity: } u_L^\star = \mathcal{U}_{\mathcal{S},L} + \left[\left(\frac{\rho_L}{\rho_L^\star}\right)\left(\frac{p^\star - p_L}{\rho_L^\star - \rho_L}\right)\right]^{1/2}, \tag{27}$$

$$\text{Right star velocity: } u_R^\star = \mathcal{U}_{\mathcal{S},R} - \left[\left(\frac{\rho_R}{\rho_R^\star}\right)\left(\frac{p^\star - p_R}{\rho_R^\star - \rho_R}\right)\right]^{1/2}. \tag{28}$$

The relations given in Eqs. (25–28) are valid for any convex EOS. It is the star-state velocity of Eq. (27) or (28) (together with star-state velocity on the other side of the contact) that is used to determine whether the overall iteration loop for the Riemann problem has converged according to the criterion discussed in §IV, and, if not, with which to update the pressure per Eqs. (18) and (19).

Once the final shock solution is computed, the shock front's speed is used to compute its position at time t as:

$$\text{Shock position:} \quad x_{\mathcal{S},\ell} = x^0_{\text{intfc}} + \mathcal{U}_{\mathcal{S},\ell} \cdot t\,, \tag{29}$$

where $\ell = L$ for a left shock front or R for a right shock front, and x^0_{intfc} is the initial location of the interface between the original left and right states.

III(b). *Rarefaction Wave Evaluation*

Consider now the case where $p^{\star(k)} \leq p_\ell$. This condition implies that there is a rarefaction wave. The head of the rarefaction is adjacent to the initial uniform state, and the tail adjoins the star-state.[12] The ODE for the characteristic through a rarefaction wave for a general convex EOS is:

$$\frac{dp}{d\rho} = a^2(\rho, p)\,, \tag{30}$$

where a is the sound speed. At the kth iterate of the overall solution loop, the initial and final conditions for this ODE are the states at the head and tail of the rarefaction:

$$\text{Initial state:} \quad p(\rho_\ell) = p_\ell \qquad\qquad \text{Final state:} \quad p(\rho^\star_\ell) = p^{\star(k)}\,. \tag{31}$$

One must numerically integrate Eq. (30) from the initial state with known pressure p_ℓ and known density ρ_ℓ, to the final state with specified pressure $p^{\star(k)}$ but *unknown* density $\rho^\star_\ell$. To be clear, in Eqs. (30–31) the quantities ρ_ℓ, p_ℓ, and $p^{\star(k)}$ are known, but $\rho^\star_\ell$ is unknown (just as in the case of a shock front). A solution to these equations is required, however, that integrates to the specified value $p^{\star(k)}$ within some specified tolerance. One way to address this problem computationally is to integrate Eq. (30) with a quadrature scheme using a constant density increment, $\Delta\rho$. This density increment modifies the independent variable (i.e., density) uniformly as one proceeds through the rarefaction in M steps in density:

$$\rho^{(0)}_\ell = \rho_\ell\,, \tag{32}$$

$$\rho^{(m)}_\ell = \rho^{(m-1)}_\ell + \Delta\rho\,, \quad m = 1, \ldots, M-1\,, \tag{33}$$

$$\rho^{(M)}_\ell \coloneqq \bar{\rho}^\star_\ell = \rho^{(M-1)}_\ell + \Delta\rho\,. \tag{34}$$

Here, the bar in $\bar{\rho}^\star_\ell$ indicates that this is a provisional value: recall that one does not know *a priori* the true value of $\rho^\star_\ell$ that integrates to the desired star-state pressure, $p^{\star(k)}$. Consequently, one does not know the correct value of $\Delta\rho$; therefore, one must solve for $\Delta\rho$ so that the desired star-state pressure is achieved.[13] Numerically integrating Eq. (30) in this fashion, a value for the pressure at $\bar{\rho}^\star_\ell$ is computed; this pressure will likely *not* equal the desired value, $p^{\star(k)}$. This computed pressure value can be used, together with the desired star-state pressure, to define a scalar function of the independent variable $\Delta\rho$ that equals the discrepancy between desired and computed star-state pressures:

$$\mathcal{R}^{(k)}(\Delta\rho) = 0 = p^{\star(k)} - \mathcal{I}(\Delta\rho; \rho_\ell, p_\ell)\,, \tag{35}$$

where $\mathcal{I}(\Delta\rho; \rho_\ell, p_\ell)$ denotes the value obtained by numerically integrating Eq. (30) to the final state, given the argument $\Delta\rho$. Solving the scalar nonlinear equation Eq. (35) to some specified accuracy determines the value of $\Delta\rho$ such that the characteristic equation integrates to the prescribed the kth-step star-state pressure.

At the mth step in density through the rarefaction, Eq. (30) can be integrated formally as

$$\int_{p(\rho_\ell^{(m-1)})}^{p(\rho_\ell^{(m)})} dp = \int_{\rho_\ell^{(m-1)}}^{\rho_\ell^{(m)}} a^2(\rho, p(\rho))\, d\rho\,, \tag{36}$$

where $\ell = L, R$. The basic fourth-order Runge-Kutta scheme for this mth integration step can be written:

$$\hat{p}^{(1)} = p^{(m-1)}\,, \qquad a^{(1)} = \mathcal{A}_\ell(\rho_\ell^{(m-1)}, \quad \hat{p}^{(1)})\,, \tag{37}$$

$$\hat{p}^{(2)} = p^{(m-1)} + \frac{1}{2}\,\Delta\rho\left(a^{(1)}\right)^2\,, \qquad a^{(2)} = \mathcal{A}_\ell(\rho_\ell^{(m-1)} + \frac{1}{2}\,\Delta\rho,\, \hat{p}^{(2)})\,, \tag{38}$$

$$\hat{p}^{(3)} = p^{(m-1)} + \frac{1}{2}\,\Delta\rho\left(a^{(2)}\right)^2\,, \qquad a^{(3)} = \mathcal{A}_\ell(\rho_\ell^{(m-1)} + \frac{1}{2}\,\Delta\rho,\, \hat{p}^{(3)})\,, \tag{39}$$

$$\hat{p}^{(4)} = p^{(m-1)} + \quad \Delta\rho\left(a^{(3)}\right)^2\,, \qquad a^{(4)} = \mathcal{A}_\ell(\rho_\ell^{(m-1)} + \quad \Delta\rho,\, \hat{p}^{(4)})\,, \tag{40}$$

$$\Rightarrow\; p^{(m)} = p^{(m-1)} + \tfrac{1}{6}\,\Delta\rho\left[\left(a^{(1)}\right)^2 + 2\left(a^{(2)}\right)^2 + 2\left(a^{(3)}\right)^2 + \left(a^{(4)}\right)^2\right], \tag{41}$$

where $\mathcal{A}_\ell(\rho, p)$ is the sound speed as a function of density and pressure for the ℓth EOS. The velocity is integrated from the appropriate second ODE in Eq. (17) as:

$$u^{(m)} = u^{(m-1)} \mp \frac{1}{6}\,\Delta\rho\left[\left(a^{(1)}/\rho_\ell^{(m-1)}\right) + 2\left(a^{(2)}/(\rho_\ell^{(m-1)} + \frac{1}{2}\,\Delta\rho)\right) + 2\left(a^{(3)}/(\rho_\ell^{(m-1)} + \frac{1}{2}\,\Delta\rho)\right) + \left(a^{(4)}/(\rho_\ell^{(m-1)} + \Delta\rho)\right)\right], \tag{42}$$

where the sign depends on the direction of the rarefaction. The corresponding spatial location for the mth integration step values is given by:

$$x_\ell^{(m)} = x_{\text{intfc}}^0 + (u^{(m)} \mp a^{(m)}) \cdot t\,, \tag{43}$$

where $a^{(m)} = \mathcal{A}_\ell(\rho^{(m)}, p^{(m)})$ is the local sound speed, and, in the $\mp$ term , "$-$" is used for left rarefactions ($\ell = L$), and "$+$" is used for right rarefactions ($\ell = R$).

From Eq. (34), the Mth (i.e., final) step of this integration corresponds to the star-state density, so that the Mth value of p from Eq. (41), the Mth value of u from Eq. (42), and the Mth value of x from Eq. (43) correspond to the associated star-state pressure, star-state velocity, and rarefaction tail position.

To summarize, the initial step of the rarefaction solution consists of using a nonlinear root solve to obtain the value of $\Delta\rho$ so that the ODE governing the flow state through the rarefaction (i.e., Eq. (30)) integrates to the proper pressure value (i.e., $p^{\star(k)}$). Once this value of $\Delta\rho$ is obtained, the star-state density and pressure for the kth iterate are known, and the remaining elements of the complete uniform star-state can be evaluated through the EOS. This star-state velocity is used, together the star-state velocity calculated for the other side of the contact, to determine if the overall iteration loop for the Riemann problem has converged and, if not, to update the pressure with Eq. (19).

After the final rarefaction solution is computed, the speeds of the rarefaction wave boundaries can be determined.[14] The velocity of the rarefaction head (adjacent to the

initial constant states) is:

$$\text{Left rarefaction head speed:} \quad \mathcal{U}_{\mathcal{H},L} = u_L - a_L \,, \tag{44}$$

$$\text{Right rarefaction head speed:} \quad \mathcal{U}_{\mathcal{H},R} = u_R + a_R \,, \tag{45}$$

where u_L and u_R are the particle velocities of the initial left and right states, and a_L and a_R are the sound speeds in those initial states. The velocity of the rarefaction tail (bordering the respective uniform star-state) is:

$$\text{Left rarefaction tail speed:} \quad \mathcal{U}_{\mathcal{T},L} = u^\star - a_L^\star \,, \tag{46}$$

$$\text{Right rarefaction tail speed:} \quad \mathcal{U}_{\mathcal{T},R} = u^\star + a_R^\star \,, \tag{47}$$

where $u^\star$ is the star-state velocity, and $a_L^\star$ and $a_R^\star$ are the sound speeds in the left and right uniform star-states, where "left" and "right" are relative to the contact discontinuity. Using these values, the positions of the rarefaction head and tail at time t are computed as:

$$\text{Rarefaction head/tail position:} \quad x_{\mathcal{B},\ell} = x^0_{\text{intfc}} + \mathcal{U}_{\mathcal{B},\ell} \cdot t \,, \tag{48}$$

where $\mathcal{B} = \mathcal{H}$ for the head or $\mathcal{T}$ for the tail, and $\ell = L$ for the left side or R for the right side.

IV. Update of the Star-State Estimates

Subsequent star-state pressure iterates are obtained from Eq. (19), and the corresponding velocity values are obtained in exactly the same manner as described in §III above. The convergence criterion for the secant iteration is that the sum of the pressure change and velocity difference is sufficiently small. Specifically, the convergence tolerance is specified for the sum of (i) the absolute difference in the estimated star-state pressure between the current and previous iterates, and (ii) the absolute difference between the left and right star-state velocities. One avoids an additional star-state evaluation step by using velocity values that are out of phase by one iteration, according to the following convergence criterion:

$$\left| \, p^{\star(k+1)} - p^{\star(k)} \, \right| + \left| \, u_L^{\star(k)} - u_R^{\star(k)} \, \right| < \epsilon \,, \tag{49}$$

where ϵ is a specified tolerance, set equal to 10^{-12} in the calculations. Although the inequality in Eq. (49) is not dimensionally consistent, it nonetheless has proven adequate for the test problems considered, where unit sets are chosen so that all final flow state quantities are nearly the same order of magnitude; it would be straightforward to consistently nondimensionalize this convergence criterion.

Once convergence is attained, the final star-state velocity is assigned as the arithmetic average of the two (nearly equal) computed values, i.e.,

$$u^\star := \frac{1}{2} \left(u_L^{\star(k)} + u_R^{\star(k)} \right) \,. \tag{50}$$

This value determines the location of the contact discontinuity at time t as:

$$\text{Contact position:} \quad x_{\mathcal{C}} = x^0_{\text{intfc}} + u^\star \cdot t \,. \tag{51}$$

Additionally, if the solution contains rarefactions, $u^\star$ is used in evaluating the rarefaction tail speeds of Eqs. (46) and (47).

V. Evaluation of the Complete Riemann Problem Solution

The procedure described in the previous sections allows one to calculate the star-state for a given Riemann problem with a general convex EOS. The final positions of key flow features are given by Eqs. (29), (48), and (51).

If there are no rarefactions in the solution, then the initial discontinuity evolves into two shock fronts, with four distinct uniform flow states, so that one can immediately assign the solution state at any position.

If there are rarefactions in the solution, then additional calculations are required to determine the solution state at specified positions in the rarefaction. This follows from the fact that the procedure of §III(b) determines the rarefaction solution at points equally spaced in density between the head and tail of the rarefaction; however, this approach affords no control of the corresponding physical locations (given in Eq. (43)). The full solution state at a specified position x in the rarefaction is evaluated numerically by interpolating to the computed state vs. x data. In the numerical examples of this report, the cubic spline routine SPLINE and association evaluation routine SEVAL of Forsythe, Malcolm, and Moler [9] is used. The last four points at either end of the rarefaction are used to fit a local cubic for the domain delimited by those points; those cubic functions are used to provide derivative information necessary for the spline interpolation in the interior of the rarefaction.

5. Examples of Solutions to the 1D Riemann Problem

In this section, we provide sample 1D Riemann problem solutions. We first consider the gamma-law gas case, the solution to which can be compared to the exact procedure for that case given by Gottlieb & Groth [14]. We then consider the highly nonlinear JWL EOS, and compare plots of computed results with those given by Shyue [28] and Lee et al. [22].[15]

5(a). Polytropic Gas Examples

We examine three polytropic gas 1D Riemann problems, the solutions to both of which are well established in the literature. The incomplete polytropic EOS used in the examples has the pressure as a function of density and SIE given as:

$$p = \mathcal{P}(\rho, e) = (\gamma - 1)\, \rho\, e\,, \tag{52}$$

where $\gamma > 1$ is the adiabatic index. For this EOS, the sound speed is given as:

$$a = \mathcal{A}(\rho, p) = \sqrt{\gamma\, p/\rho}\,. \tag{53}$$

These are the only problem-dependent functional relationships required to complete the numerical approach outlined in the previous sections.

5(a)i. *Sod Shock Tube*

The Sod shock tube problem [30] is the *de facto* minimal acceptance test for any compressible flow solver. It consists of the initial conditions given Table 1, run on the domain $0 \leq x \leq 1$, and leads to the canonical Rarefaction-Contact-Shock structure. Figure 2 displays two columns of plots for this problem, each calculated with 100 equal intervals between $x = 0$ cm and $x = 1$ cm: the left column shows results computed by a dedicated gamma-law gas Riemann solver code [17] based on the method described by Gottlieb & Groth [14], and the right column contains the same plots but with results computed by the general EOS method described in this note. The dedicated gamma-law result uses 100 steps in x through the rarefaction, while the general EOS method uses 100 steps in ρ for the integration through the rarefaction; in both cases, the rarefaction results are interpolated with a standard cubic spline routine to the appropriate subset of the cell-centered positions of the 100 spatial intervals between $x = 0$ and $x = 1$. These results are visually indistinguishable, offering compelling qualitative evidence that the general EOS code is consistent with the dedicated gamma-law gas solver.

The first column of Fig. 3 provides quantitative comparisons of these calculations with plots of the pointwise difference of the two solutions (gamma-law results minus general EOS method results). The $O(10^{-4})$ discrepancy of this difference is certainly plausible: although the secant iteration is converged to 10^{-12} in the sum of the difference between the two star-state pressures and the difference in subsequent iterates of the star-state velocity, one should not infer that the accuracy of the overall solution is of that order. This point is further illustrated in the second column in Fig. 3, which contains plots of the difference of the same dedicated gamma-law solver but with the general EOS exact solver when 1000 steps in density are used in the integration of rarefaction. All other parameters in both calculations are identical, e.g., values are plotted at the cell centers of the 100 zones between $x = 0$ and $x = 1$. The approximately factor-of-10 difference between the results in the right and left columns correlates well with the increased resolution in the rarefaction integration. It is unclear what may be the cause of the sawtooth-pattern discrepancy most evident in the pressure difference plot (third from the top, right column). From this figure, it is plausible to conclude that a more accurate solution obtains with the general EOS method solver when the integration through the rarefaction is well resolved.

x^0_{intfc} cm	t_{fin} s	γ_L –	ρ_L g/cm^3	p_L dyn/cm^2	u_L cm/s	γ_R –	ρ_R g/cm^3	p_R dyn/cm^2	u_R cm/s
0.5	0.25	1.4	1.0	1.0	0	1.4	0.125	0.1	0

Table 1: Initial conditions for the Sod shock tube problem.

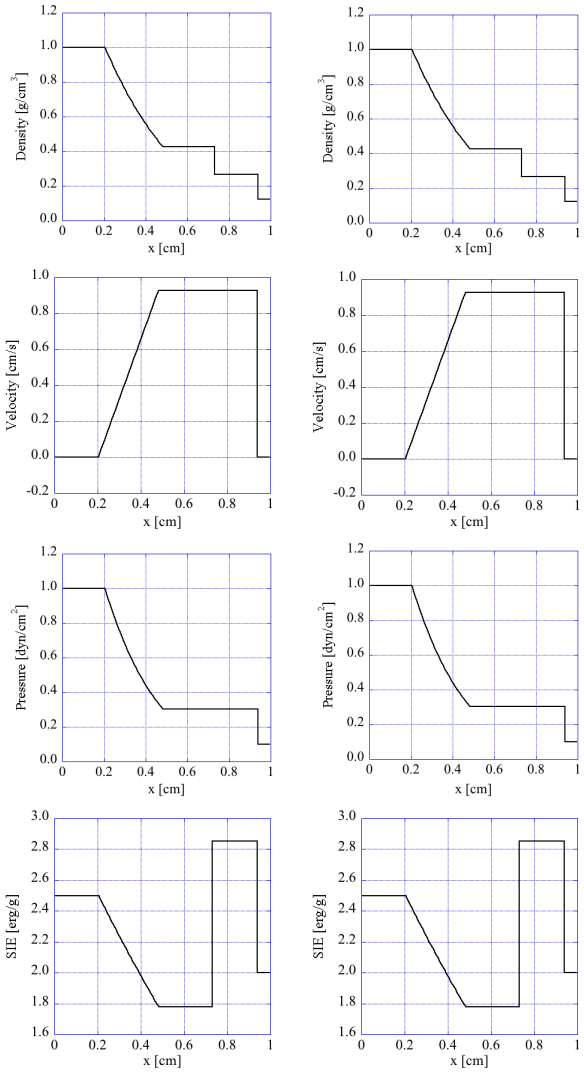

Figure 2: Results for the Sod problem [30] as specified in Table 1 for, from top to bottom, density, velocity, pressure, and SIE. The left column shows the results with a dedicated gamma-law-gas Riemann solver [17], and the right column shows the results with the general EOS exact solution code described in this report. Values are plotted at the cell centers of the 100 zones between $x = 0$ and $x = 1$. The results of the two methods are qualitatively indistinguishable.

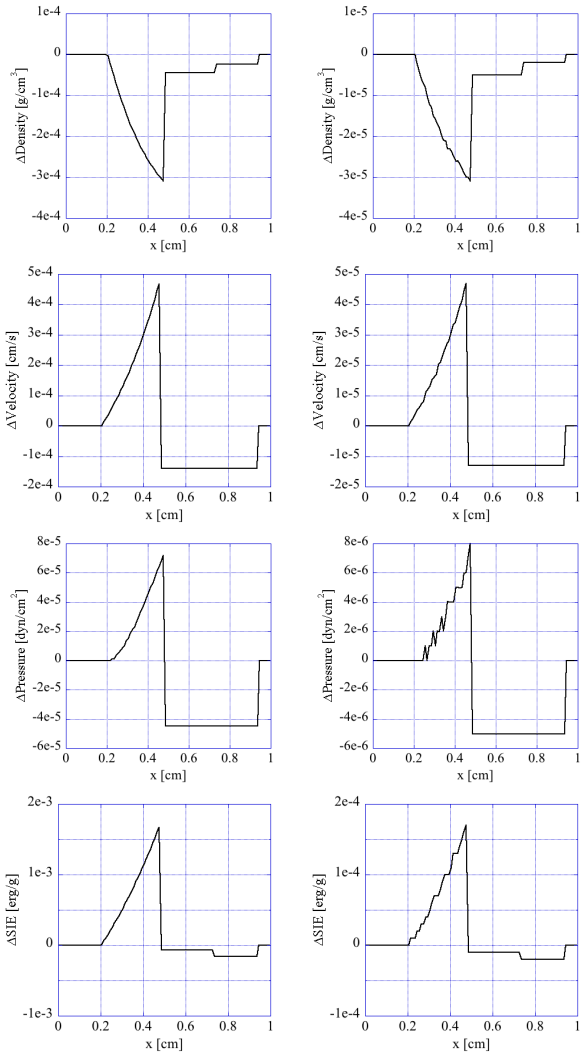

Figure 3: Plots of the pointwise differences between results of a dedicated gamma-law-gas Riemann solver [17] and the general EOS exact solution code described in this report for the Sod problem [30]. The left column shows the difference when 100 steps in density are used in the integration of the general EOS exact solver (i.e., using the data plotted in Fig. 2), and the right column shows the difference when 1000 steps in density are used in the same integration. All other parameters in both calculations are identical, e.g., results are plotted at the cell centers of the 100 zones between $x = 0$ and $x = 1$. The approximately factor-of-10 difference in discrepancies correlates very well with the increased resolution in the rarefaction integration.

5(a)ii. *Reversed Sod Shock Tube*

The reversed Sod shock tube problem is based on the Sod problem, but with the left and right initial states interchanged, thereby leading to a Shock-Contact-Rarefaction solution. This problem tests the ability of the general EOS code to resolve shocks and rarefactions of opposite orientation to those of the Sod problem. The initial conditions given Table 2. Graphical results are presented in Fig. 4, the two leftmost columns of which contain the plots equivalent to those for the Sod problem in Fig. 2, while the rightmost column contains the difference between the values plotted in the same row (i.e., results analogous to the left column of Fig. 3). These plots suggest that the general EOS code resolves left-facing shocks and right-facing rarefactions with accuracy comparable to that of the right-facing shock and left-facing rarefaction of §5(a)i.

x^0_{intfc} cm	t_{fin} s	γ_L –	ρ_L g/cm^3	p_L dyn/cm^2	u_L cm/s	γ_R –	ρ_R g/cm^3	p_R dyn/cm^2	u_R cm/s
0.5	0.25	1.4	0.125	0.1	0	1.4	1.0	1.0	0

Table 2: Initial conditions for the reversed Sod shock tube problem.

5(a)iii. *Modified Sod Shock Tube*

The modified Sod shock tube problem [40] is based on the Sod problem, but with the material to the left of the initial discontinuity being a polytropic gas having a different adiabatic exponent and different initial conditions. This problem, which has an exact solution with the standard gamma-law gas Riemann solver, tests the ability of the general EOS code to work with two EOSs. The initial conditions are given Table 3. Graphical results are presented in Fig. 5, the two leftmost columns of which contain the plots equivalent to those for the Sod problem in Fig. 2, while the rightmost column contains the difference between the values plotted in the same row (i.e., results analogous to the left column of Fig. 3). These plots suggest that the general EOS code solves this multi-material, polytropic gas Rarefaction-Contact-Shock problem with accuracy comparable to that of the Sod and reversed Sod problems of the previous sections.

x^0_{intfc} cm	t_{fin} s	γ_L –	ρ_L g/cm^3	p_L dyn/cm^2	u_L cm/s	γ_R –	ρ_R g/cm^3	p_R dyn/cm^2	u_R cm/s
0.5	0.2	2.0	1.0	2.0	0	1.4	0.125	0.1	0

Table 3: Initial conditions for the modified Sod shock tube problem.

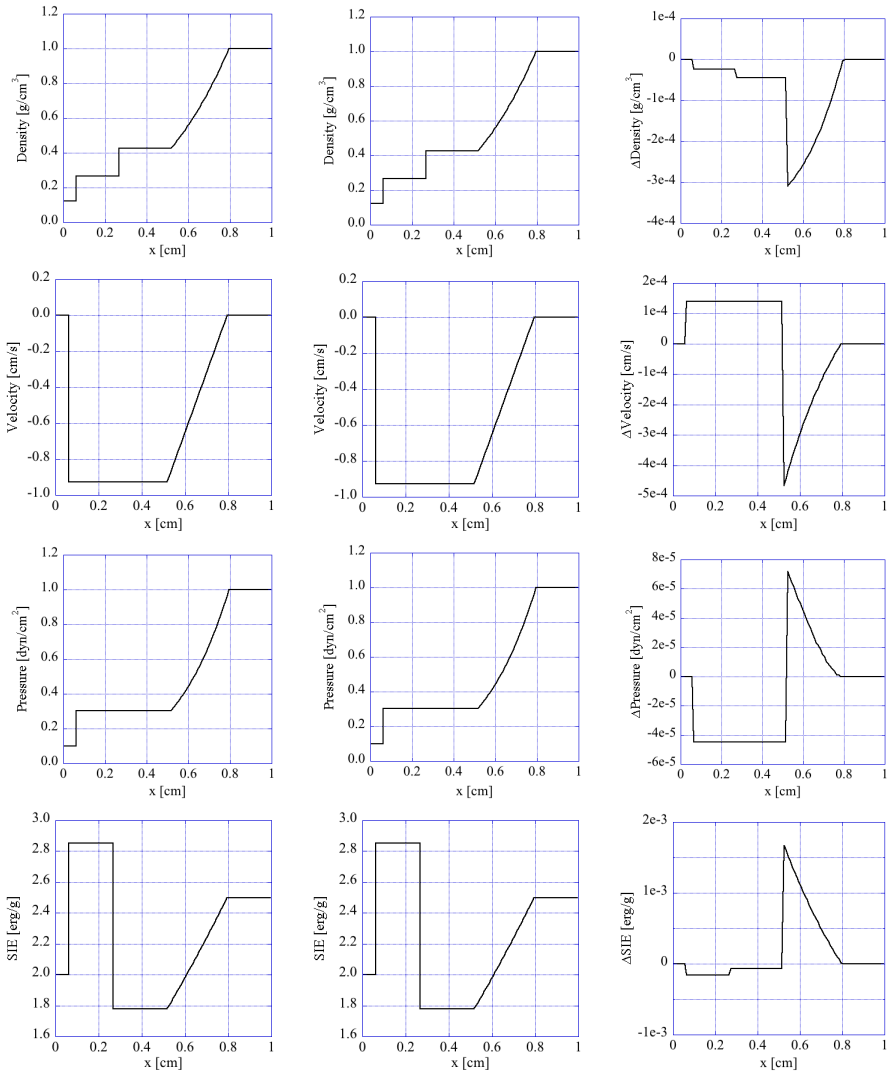

Figure 4: Results for the reversed Sod problem as specified in Table 2 for, from top to bottom, density, velocity, pressure, and SIE. The left column shows the results with a dedicated gamma-law-gas Riemann solver [17]; the middle column shows the results with the general EOS exact solution code described in this report; and the right column contains the pointwise difference of the data in the previous two columns, plotted at the cell centers of the 100 zones between $x = 0$ and $x = 1$.

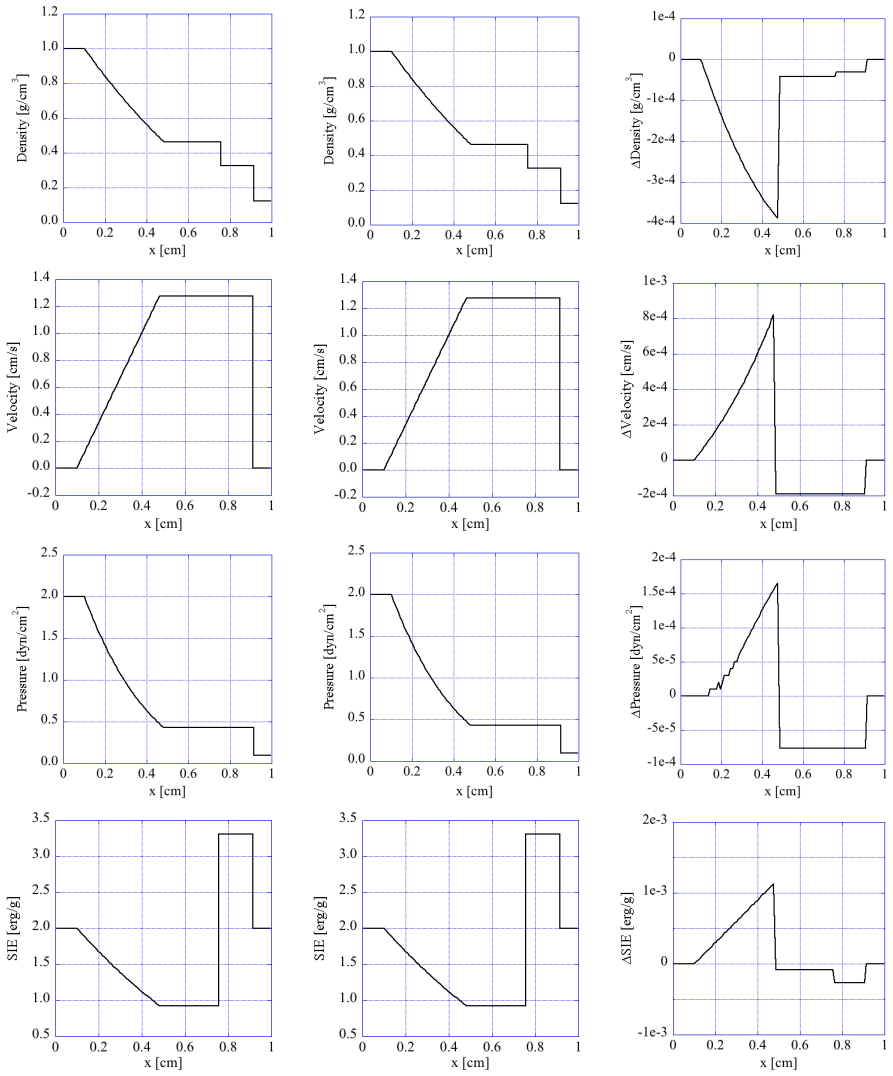

Figure 5: Results for the modified Sod problem as specified in Table 3 for, from top to bottom, density, velocity, pressure, and SIE. The left column shows the results with a dedicated gamma-law-gas Riemann solver [17]; the middle column shows the results with the general EOS exact solution code described in this report; and the right column contains the pointwise difference of the data in the previous two columns, plotted at the cell centers of the 100 zones between $x = 0$ and $x = 1$.

5(b). JWL EOS Examples

We examine two JWL EOS 1D Riemann problems, graphical results for which are available in the literature. According to Dobratz [8], "The Jones-Wilkins-Lee (JWL) equation of state has been used to describe accurately the pressure-volume-energy behavior of the detonation products of explosives in applications of metal acceleration." There are countless references for this EOS; a particularly concise and useful account is given by Weseloh [37]. Following Lee et al. [22], the JWL EOS is commonly written in the form

$$p = \mathcal{P}(\rho, e) = \Gamma\,\rho\,e + A\left(1 - \frac{\Gamma}{R_1}\frac{\rho}{\rho_0}\right)\exp\left(-R_1\,\frac{\rho_0}{\rho}\right) + B\left(1 - \frac{\Gamma}{R_2}\frac{\rho}{\rho_0}\right)\exp\left(-R_2\,\frac{\rho_0}{\rho}\right), \tag{54}$$

where the constants (and their dimensions in HE units[16]) associated with a particular material are: (i) reference mass density ρ_0 (g cm^{-3}); (ii) low-pressure Grüneisen coefficient $\Gamma > 0$ (dimensionless); (iii) high-pressure coefficients A (Mbar) and R_1 (dimensionless); and (iv) intermediate-pressure coefficients B (Mbar) and R_2 (dimensionless). In this description, the terms low-, intermediate-, and high-pressure refer to approximate domains where the corresponding terms dominate the JWL pressure.

As discussed by Lee et al. [22], the relation in Eq. (54) can be written in the general Mie-Grüneisen form

$$p = \mathcal{P}(\rho, e) = \Gamma\,\rho\,(\,e - e_{\mathsf{ref}}(\rho)\,) + p_{\mathsf{ref}}(\rho)\,, \tag{55}$$

where $e_{\mathsf{ref}}(\rho)$ and $p_{\mathsf{ref}}(\rho)$ are a reference state curve, which, when chosen as an isentrope, reduces the above expression to the sum of the usual ideal gas EOS and an additional term:

$$p = \mathcal{P}(\rho, e) = \Gamma\,\rho\,e + f(\rho) \quad \text{where} \tag{56}$$

$$f(\rho) \coloneqq A\left(1 - \frac{\Gamma}{R_1}\frac{\rho}{\rho_0}\right)\exp\left(-R_1\,\frac{\rho_0}{\rho}\right) + B\left(1 - \frac{\Gamma}{R_2}\frac{\rho}{\rho_0}\right)\exp\left(-R_2\,\frac{\rho_0}{\rho}\right). \tag{57}$$

This representation leads to a compact expression for the square of the sound speed (see Eq. (5)) as

$$a^2 = \mathcal{A}^2(\rho, p) = (\Gamma + 1)p/\rho - f(\rho)/\rho - f\,'(\rho)/\rho^2\,, \tag{58}$$

where the first term on the RHS is identical to the square of the polytropic gas sound speed of Eq. (53).

5(b)i. *Shyue Shock Tube*

This problem, used by Shyue [28] as a test problem in algorithm development, uses the same JWL EOS on either side of a massless discontinuity. The JWL parameters, listed in Table 4, are an approximation for the EOS of TNT. This problem is run on the interval $0 \le x \le 100$ cm, with the initial conditions given in Table 5. Although no

exact solution is reported in [28], graphical results of the compressible flow simulation of this problem are provided.

Results for this problem are given in Fig. 6, which contains snapshot plots of the density, velocity, pressure, and SIE. The left column contains results from the general EOS exact solution code described in this report, and the right column plots are from Shyue [28]; the plots from [28] do not include an exact solution evaluation but include, instead, a highly resolved calculation, plotted as a solid line (Shyue does not provide SIE results). Based on these graphical results, the exact solution code appears to be consistent with the published results. Quantitative confirmation of the exact solution code correctness would be desirable, but is not available from this comparison.

JWL EOS	HE	ρ_0 g/cm^3	e_0 Mbar-cm^3/g	Γ_0 –	A Mbar	B Mbar	R_1 –	R_2 –
#1	TNT	1.84	0.0	0.25	8.545	0.205	4.6	1.35

Table 4: JWL parameters for TNT used in the Shyue shock tube problem.

JWL EOS	x^0_{intfc} cm	t_{fin} μs	ρ_L g/cm^3	p_L Mbar	u_L cm/μs	ρ_R g/cm^3	p_R Mbar	u_R cm/μs
#1	50	12	1.7	10.0	0.0	1.0	0.5	0.0

Table 5: Initial conditions for the Shyue shock tube problem, using the JWL EOS parameters given in Table 4.

5(b)ii. *Lee Shock Tube*

Lee et al. [22] consider another JWL 1D Riemann problem and do provide graphical exact solution results. As in the previous problem, the same JWL EOS is used on either side of the initial discontinuity. The JWL parameters, listed in Table 6, are an approximation for the EOS of LX-17. Like the previous example, this problem is also run on the interval $0 \leq x \leq 100$ cm, but with the different initial conditions, as given in Table 7. This configuration is a slight modification of a problem run by Banks [2].

Results for this problem are given in Fig. 7, which contains snapshot plots of the density, velocity, pressure, and SIE. The plots in the left column are from the general EOS exact solution code described in this report, while the plots in the right column are from Lee et al. [22], which includes an exact solution evaluation (in red) together with compressible flow simulation results using different methods (Lee et al. do not provide SIE results). Based on these graphical results, it appears that the exact solution code results are completely consistent with those of Lee et al. Again, quantitative confirmation of the exact solution code correctness would be desirable, but is not available from this comparison.

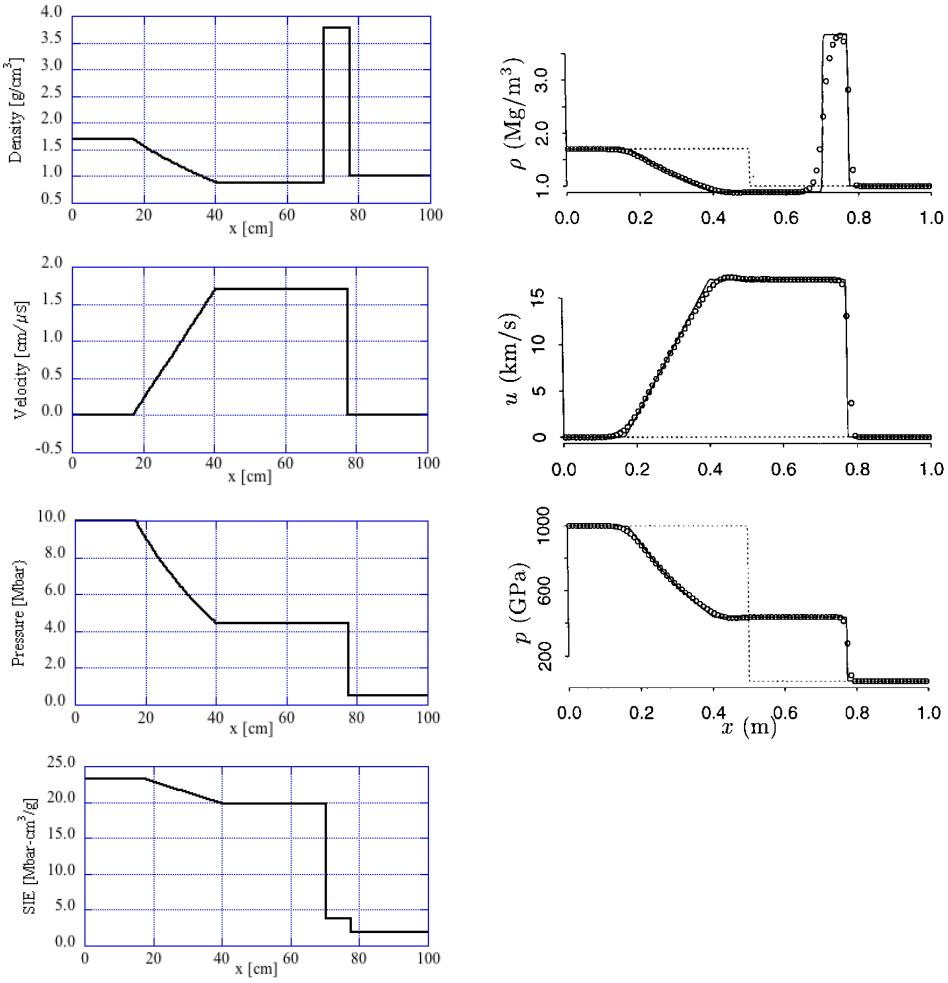

Figure 6: Results for the problem of Shyue [28] as specified in Table 5 for, from top to bottom, density, velocity, pressure, and SIE. The left column shows the results with the general EOS exact solution code described in this report, and the right column contains the published results from [28] (Shyue does not provide SIE results) in which the solid line denotes a highly refined computed (not exact) result.

6. Summary

This report contains a description of an algorithm with which to compute the complete numerical solution of the one-dimensional, Cartesian Riemann problem for compressible flow with general, convex equations of state. Based on several published works, this note motivates and documents the approach used in the source code that evaluates solutions for the 1D, Cartesian Riemann problem with a JWL equation of state in the

JWL EOS	HE	ρ_0 g/cm^3	e_0 Mbar-cm^3/g	Γ_0 –	A Mbar	B Mbar	R_1 –	R_2 –
#2	LX-17	1.905	0.0	0.8938	632.1	-0.04472	11.3	1.13

Table 6: JWL parameters for TNT used in the Lee shock tube problem.

JWL EOS	x^0_{intfc} cm	t_{fin} μs	ρ_L g/cm^3	p_L Mbar	u_L cm/μs	ρ_R g/cm^3	p_R Mbar	u_R cm/μs
#2	50	20	0.9525	1.0	0.0	3.810	2.0	0.0

Table 7: Initial conditions for the Lee shock tube problem, using the JWL EOS parameters given in Table 6.

ExactPack package [16, 29]. The numerical results given for problems with either a polytropic gas EOS or the JWL EOS provide, respectively, quantitative and qualitative evidence that the method and associated software generate accurate solutions for the problems considered.

Acknowledgements

This work was performed under the auspices of the United States Department of Energy by Los Alamos National Security, LLC, at Los Alamos National Laboratory under contract DE-AC52-06NA25396. The author gratefully acknowledges the Verification Project (part of the LANL ASC V&V Program Element) and Project Leader Scott Doebling for the support of this work, and thanks Bob Singleton for carefully reviewing a draft of this manuscript. This report is available as Los Alamos National Laboratory report LA-UR-15-XXXXX.

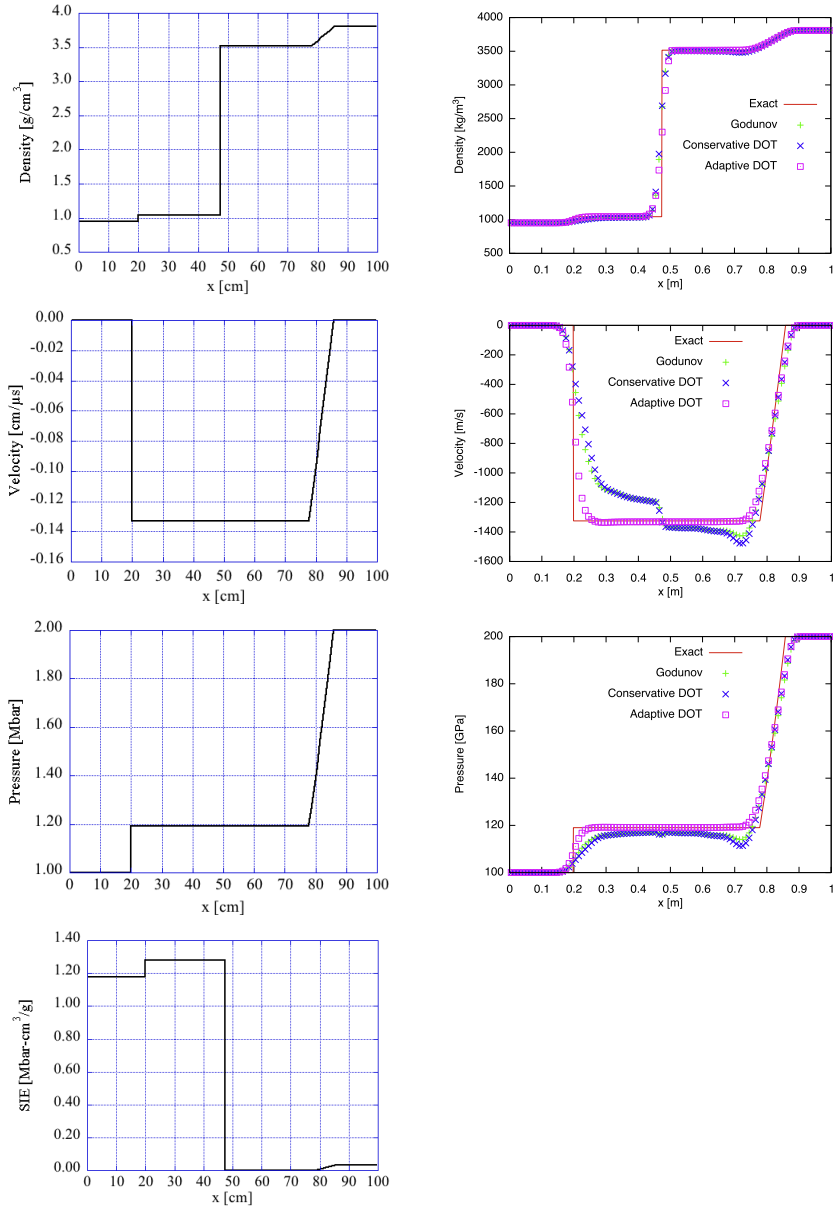

Figure 7: Results for the problem of Lee et al. [22] as specified in Table 7 for, from top to bottom, density, velocity, pressure, and SIE. The left column shows the results with the general EOS exact solution code described in this report, and the right column contains the published plots from [22] (Lee et al. do not provide SIE results), in which the red line denotes Lee et al.'s exact results from [22].

References

[1] M. Arienti, E. Morano, and J.E. Shepherd. Shock and detonation modeling with the Mie-Grüneisen equation of state. Technical Report FM99-8, Graduate Aeronautical Laboratories, California Institute of Technology, 1999. URL: http://shepherd.caltech.edu/EDL/publications/reprints/galcit_fm99-8.pdf.

[2] J.W. Banks. On exact conservation for the Euler equations with complex equations of state. *Communications in Computational Physics*, 8:995–1015, 2010. doi:10.4208/cicp.090909.100310a.

[3] H.A. Bethe. Report on "The theory of shock waves for an arbitrary equation of state". Technical Report PB-32189, Air Force Weapons Laboratory, 1942. Clearinghouse for Federal Scientific and Technical Information, U.S. Department of Commerce, Washington, D.C.

[4] A. Bressan. Hyperbolic conservation laws: An illustrated tutorial. In L. Ambrosio, A. Bressan, D. Helbing, A. Klar, E. Zuazua, B. Piccoli, and M. Rascle, editors, *Modelling and Optimisation of Flows on Networks*, volume 2062 of *Springer Lecture Notes in Mathematics, C.I.M.E. Foundation Subseries*, pages 157–245. Springer Verlag, 2013. An earlier version is available at the indicated website. URL: http://ima.umn.edu/2008-2009/SP7.13-31.09/activities/Bressan-Alberto/HCL_lecture_notes.pdf.

[5] P. Colella and H.M. Glaz. Efficient solution algorithms for the Riemann problem for real gases. *Journal of Computational Physics*, 59:264–289, 1985. doi:10.1016/0021-9991(85)90146-9.

[6] R. Courant and K.O. Friedrichs. *Supersonic Flow and Shock Waves*. Springer-Verlag, 1976.

[7] W. Dahmen, S. Müller, and A. Voß. Riemann problem for the Euler equation with non-convex equation of state including phase transitions. In G. Warnecke, editor, *Analysis and Numerics for Conservation Laws*, pages 137–162. Springer-Verlag, 2006. doi:10.1007/3-540-27907-5.

[8] B.M. Dobratz. Properties of chemical explosives and explosive simulants. Technical Report UCRL-51319 Rev. 1, Lawrence Livermore Laboratory, 1974.

[9] G.E. Forsythe, M.A. Malcolm, and C.B. Moler. *Computer Methods for Mathematical Computations*. Wiley, 1977.

[10] B. Fryxell, K. Olson, P. Ricker, F.X. Timmes, M. Zingale, D.Q. Lamb, P. MacNeice, R. Rosner, J.W. Truran, and H. Tufo. FLASH: An adaptive mesh hydrodynamics code for modeling astrophysical thermonuclear flashes. *The Astrophysical Journal Supplement Series*, 131:273–334, 2000. doi:10.1086/317361.

[11] F.R. Gilmore. Equilibrium composition and thermodynamic properties of air to 24,000°K. Technical Report RM-1543, The RAND Corporation, 1955. URL: http://www.rand.org/content/dam/rand/pubs/research_memoranda/2008/RM1543.pdf.

[12] S.K. Godunov. A difference method for the numerical calculation of discontinuous solutions of hydrodynamic equations. *Matematischeskiy Sbornik*, 47(89):271–306, 1959. In Russian. URL: http://www.mathnet.ru/links/b783eef8b6479b2ffe3c42511559ec8c/sm4873.pdf.

[13] S.K. Godunov. A difference method for the numerical calculation of discontinuous solutions of hydrodynamic equations. Technical Report JPRS: 7225, U.S. Joint Publications Research Service, 1960. Available through the U.S. Dept. of Commerce, Office of Technical Services.

[14] J.J. Gottlieb and C.P.T. Groth. Assessment of Riemann solvers for unsteady one-dimensional inviscid flows of perfect gases. *Journal of Computational Physics*, 78:437–458, 1988. doi:10.1016/0021-9991(88)90059-9.

[15] O. Heuzé, S. Jaouen, and H. Jourdren. Dissipative issue of high-order shock capturing schemes with non-convex equations of state. *Journal of Computational Physics*, 228:833–860, 2009. doi:10.1016/j.jcp.2008.10.005.

[16] D.M. Israel, R.L. Singleton, Jr., S.W. Doebling, and J.R. Kamm. ExactPack v1.0. Technical Report LA-CC-14-047, Los Alamos National Laboratory, 2014.

[17] J.R. Kamm. SHKTUB: A polytropic gas Riemann solver code. Unpublished source code, 2014.

[18] L.D. Landau and E.M. Lifschitz. *Course of Theoretical Physics, Volume 6: Fluid Mechanics*. Pergamon Press, 1978.

[19] C.B. Laney. *Computational Gasdynamics*. Cambridge University Press, 1998.

[20] M. Larini, R. Saurel, and J.C. Loraud. An exact Riemann solver for detonation products. *Shock Waves*, 2:225–236, 1992. doi:10.1007/BF01414758.

[21] P.D. Lax. *Hyperbolic Systems of Conservation Laws and the Mathematical Theory of Shock Waves*. SIAM, 1973.

[22] B.J. Lee, E.F. Toro, C.E. Castro, and N. Nikiforakis. Adaptive Osher-type scheme for the Euler equations with highly nonlinear equations of state. *Journal of Computational Physics*, 246:165–183, 2013. doi:10.1016/j.jcp.2013.03.046.

[23] R.J. LeVeque. *Finite Volume Methods for Hyperbolic Problems*. Cambridge University Press, 2005.

[24] H.W. Liepmann and A. Roshko. *Elements of Gasdynamics*. John Wiley & Sons, 1957.

[25] R. Menikoff and B.J. Plohr. The Riemann problem for fluid flow of real materials. *Reviews of Modern Physics*, 61:75–130, 1989. doi:10.1103/RevModPhys.61.75.

[26] S. Müller and A. Voß. Riemann problem for the Euler equation with nonconvex and nonsmooth equation of state: Construction of wave curves. *SIAM Journal of Scientific Computing*, 28:651–681, 2006. doi:10.1137/040619909.

[27] L. Quartapelle, L. Castelletti, A. Guardone, and G. Quaranta. Solution of the Riemann problem of classical gasdynamics. *Journal of Computational Physics*, 190:118–140, 2003. doi:10.1016/S0021-9991(03)00267-5.

[28] K.-M. Shyue. A fluid-mixture type algorithm for compressible multicomponent flow with Mie-Grüneisen equation of state. *Journal of Computational Physics*, 171:678–707, 2001. doi:10.1006/jcph.2001.6801.

[29] R.L. Singleton, Jr., S.W. Doebling, D.M. Israel, and J.R. Kamm. ExactPack: A master code of exact solutions for code verification. Technical Report LA-UR-15-20463, Los Alamos National Laboratory, 2015.

[30] G.A. Sod. A survey of several finite difference methods for systems of nonlinear hyperbolic conservation laws. *Journal of Computational Physics*, 27:1–31, 1978. doi:10.1016/0021-9991(78)90023-2.

[31] P.A. Thompson. *Compressible-Fluid Dynamics*. Hamilton Press, 1988.

[32] P.A. Thompson and K. C. Lambrakis. Negative shock waves. *Journal of Fluid Mechanics*, 60:187–208, 1973. doi:10.1017/S002211207300011X.

[33] E.F. Toro. *Riemann Solvers and Numerical Methods for Fluid Dynamics*. Springer-Verlag, 1997.

[34] J.A. Trangenstein. *Numerical Solution of Hyperbolic Partial Differential Equations*. Cambridge University Press, 2009.

[35] B. Wendroff. The Riemann problem for materials with nonconvex equations of state I: Isentropic flow. *Journal of Mathematical Analysis and Applications*, 38:454–466, 1972. doi:10.1016/0022-247X(72)90103-5.

[36] B. Wendroff. The Riemann problem for materials with nonconvex equations of state II: General flow. *Journal of Mathematical Analysis and Applications*, 38:640–658, 1972. doi:10.1016/0022-247X(72)90075-3.

[37] W. Weseloh. JWL in a Nutshell. Technical Report LA-UR-14-24318, Los Alamos National Laboratory, 2014.

[38] G.B. Whitham. *Linear and Nonlinear Waves*. Wiley & Sons, 1974. This book is legally available online at the indicated website. URL: https://archive.org/details/LinearAndNonlinearWaves.

[39] Wikipedia. Secant method — Wikipedia, The Free Encyclopedia, 2014. [Online; accessed 17-December-2014]. URL: http://en.wikipedia.org/w/index.php?title=Secant_method&oldid=636742597.

[40] Y.B. Yanilkin, E.A. Goncharov, V.Yu. Kolobyanin, V.V. Sadchikov, J.R. Kamm, M.J. Shashkov, and W.J. Rider. Multi-material pressure relaxation methods for Lagrangian hydrodynamics. *Computers & Fluids*, 83:137–143, 2013. doi:10.1016/j.compfluid.2012.05.020.

[41] Y.B. Zel'dovich and Y.P. Raizer. *Physics of Shock Waves and High-Temperature Hydrodynamic Phenomena*. Academic Press, 1966.

Notes

[1]Per [25], the fundamental derivative is defined as

$$\mathcal{G} \coloneqq -(1/2)V\left[(\partial^2 p/\partial V^2)_s/(\partial p/\partial V)_s\right]$$

where $V \coloneqq 1/\rho$ is the specific volume and s is the entropy. The fundamental derivative "measures the convexity of the isentropes in the p–V plane [31]."

[2]Understanding the characteristic form of the Euler equations—or, more generally, of hyperbolic conservation laws—is indispensable for comprehending the structure of the solution to the 1D Riemann problem. This important topic is beyond the scope of the present report. Among the manuscripts that cover this topic are: for the Euler equations of gas dynamics the book by Courant and Friedrichs [6] is the definitive reference, with the masterful monograph of Whitham [38] (in particular, Chapters 5 and 6) running a close second, while the more modern, numerically-oriented texts of Laney [19], LeVeque [23], and Trangenstein [34] offer less comprehensive treatments of this particular aspect; for general systems of hyperbolic conservation laws, the tour de force of Lax [21] is required reading, while the article by Bressan [4] provides an approachable introduction.

[3]The topic of non-convex EOSs is discussed, e.g., by Bethe [3], Wendroff [35, 36], Dahmen et al. [7], and Müller and Voß [26]. An analytic, non-convex EOS for the fictitious material "Bizarrium" is described by Heuzé et al. [15], who examine a 1D Riemann problem for that material.

[4]There likely is an initial discontinuity in entropy across the contact that persists through the solution. According to LeVeque [23], "The contact discontinuity is also sometimes called the *entropy wave*, since it carries a jump in entropy." Since there is no mass flux through the contact wave, however, that entropy discontinuity is not the result of any process *through* the wave.

[5]"The side of the shock front through which the gas enters the shock front was called the *front side* or the side ahead of the shock front. The other side was called the *back side*. In other words, the particles cross the shock front from the front toward the back side. . . It should be clearly understood that the direction in which the shock front *moves*, given the sign of [*the shock velocity*] $\mathcal{U}$, has nothing to do with the direction toward which it *faces*, i.e., with the distinction between the front and back side of the shock which depends only on the relative velocity v. Whether the front advances, is stationary, or recedes, depends on the absolute velocity." [6], §57.

[6]If a rarefaction exists to the left of the contact discontinuity for $t > 0$, it is called a *left-facing* rarefaction. Similarly, a rarefaction to the right of the contact for $t > 0$, it is called a *right-facing* rarefaction.

[7]It was perhaps Godunov [12, 13] who published the first iterative scheme with which to solve the 1D Riemann problem for a polytropic gas.

[8]Banks [2] provides a description (lacking a few details needed for implementation) of a Riemann solver for the JWL EOS. Fryxell et al. [10] describe the Colella and Glaz

procedure as applied to polytropic gases. Larini et al. [20] focus on EOSs of the form $p = p(\rho, T)$ and apply their method to a fifth-order virial EOS. Arienti et al. [1] give a limited description of a solution procedure for the Mie-Grüneisen EOS tailored to their specific problems. Lee et al. [22] use a JWL EOS in Mie-Grüneisen form and develop their approach accordingly. Quartapelle et al. [27] develop a derivative-based Newton-method based approach and apply it to more complicated polytropic and *non*-polytropic van der Waals EOSs.

[9]The ZEROIN routine of Forsythe, Malcolm, and Moler [9] was chosen because (i) it only uses function calls (i.e., no derivative information is needed), and (ii) it is both robust and efficient (by using the original Brent's method, which combines the bisection with the secant method and inverse quadratic interpolation). For input, however, this routine requires two abscissæ that bracket the root, i.e., give function values of opposite sign. In principle, this should be straightforward, but, given the nonlinearity of the functions to which it is applied and the nonlinearity of the EOSs used, this initially proved problematic. A simple method was devised that, in conjunction with ZEROIN, was used to determine initial abscissae that bracketed the root. The key idea is that, if two initial values were of the same sign, then those values were used to estimate an abscissa value at which the linear extrapolation of the function would be zero. (Given the intrinsic nonlinearities, in practice this was never the case.) The pair of abscissae for the next iterate were taken to be (1) the abscissa (of the previous two) that had the smallest absolute function value, and (2) the extrapolated abscissa value. For the problems considered in this report, this simple algorithm was able to bracket the root for all ZEROIN calls in less than six iterations.

[10]The secant method differs from the Newton-method based approach of Quartapelle et al. [27], who formulate a pair of equations in two unknowns taken to be the specific volumes (i.e., inverse density) in the two star-states to the left and right of the contact discontinuity. The use by Quartapelle et al. of Newton's method requires the evaluation of derivatives, which those authors evaluate analytically for the van der Waals gas EOSs that they consider. The closed-form expressions for those derivative terms are quite complicated.

[11]Colella & Glaz [5] denote the mean Lagrangian wave speed W, as in their Eq. (16).

[12]More precisely, "An expansion wave is composed of characteristics; in particular, the boundaries $b_1(t)$ and $b_2(t)$ are characteristics. The boundary on the high-pressure side is called the *head* of the expansion. Similiarly, the boundary on the low-pressure side is called the *tail* of the expansion." [19]

[13]For the EOSs considered, this density increment is negative, i.e., $\Delta\rho < 0$, since the integration proceeds from the high-pressure, high-density uniform state to the lower-pressure, lower-density, post-rarefaction star-state.

[14]"The [*rarefaction*] wave has a fan-type shape and is enclosed by two bounding characteristics corresponding to the Head and the Tail of the wave." [33], §3.1.3. For the left- and right-facing rarefactions waves discussed in the text, those bounding characteristics propagate at the velocities indicated in Eqs. (44–47). In the case of a γ-law gas, §4.2.2 and §4.2.4 of [33] contain derivations of the complete solution through,

respectively, left and right rarefactions.

[15]Colella and Glaz [5] provide results for an interesting 1D Riemann test problem involving air and a JWL EOS; unfortunately, these authors do not provide all of the information required to replicate their calculations. Additionally, the EOS of air used in this problem is that of Gilmore, the cited report of whom [11] is a detailed study of different representations for the EOS for air. It is unclear from this report and from the Colella and Glaz paper *exactly* what representation for the air EOS was used in [5], rendering comparison with those results problematic.

[16]HE units are a consistent set of units well suited to HE phenomena and consist of the following: mass in g, length in cm, time in μs, and pressure in Mbar (1 Mbar = 100 GPa), so that mass density is in g cm^{-3}, velocity is in cm μs^{-1}, and SIE is in Mbar cm^3 g^{-1}.